

Laser Cooling and Magnetic Trapping at Several Tesla

J. R. Guest,* J.-H. Choi, E. Hansis, A. P. Povilus, and G. Raithel

FOCUS Center, Department of Physics, University of Michigan, Ann Arbor, Michigan 48109-1120, USA

(Received 29 September 2004; published 23 February 2005)

Laser cooling and magnetic trapping of ^{85}Rb atoms have been performed in extremely strong and tunable magnetic fields, extending these techniques to a new regime and setting the stage for a variety of cold atom and plasma experiments. Using a superconducting Ioffe-Pritchard trap and an optical molasses, 2.4×10^7 atoms were laser cooled to the Doppler limit and magnetically trapped at bias fields up to 2.9 T. At magnetic fields up to 6 T, 3×10^6 cold atoms were laser cooled in a pulsed loading scheme. These bias fields are well beyond an order of magnitude larger than those in previous experiments. Loading rates, molasses lifetimes, magnetic-trapping times, and temperatures were measured using photoionization and electron detection.

DOI: 10.1103/PhysRevLett.94.073003

PACS numbers: 32.80.Pj, 32.80.Lg

Laser-cooling and magnetic-trapping methodologies have revolutionized atomic physics in recent years, paving the way for the realization of Bose-Einstein condensation [1] and opening up new regimes in collision physics [2], high-precision spectroscopy [3], and plasma physics [4]. In most of these experiments, electromagnetic coils have been used to generate shallow traps with modest bias magnetic fields that inhibit Majorana flops [5] and thereby reduce trap loss. Permanent [6] and superconducting magnets [7,8] have been used to develop deeper magnetic traps with bias magnetic fields up to 0.16 T [7].

In this Letter, we report on laser cooling in variable magnetic fields up to 6 T and magnetic trapping at fields up to 2.9 T in a superconducting Ioffe-Pritchard trap. While our results open multiple research frontiers, strong-magnetic-field neutral-atom traps may have the largest impact on cold Rydberg gas and plasma studies. Low magnetic-field experiments on these systems have been performed in magneto-optical traps [4]. In strong magnetic fields, the bound electron cyclotron radius can be less than the size of Rydberg atoms (10^3 – $10^4 a_0$ where a_0 is the Bohr radius), at which point the internal dynamics of Rydberg atoms are fundamentally altered. Strongly magnetized high-angular momentum Rydberg atoms, unlike their chaotic low-angular momentum counterparts [9], are expected to support regular orbits [10] and have exceptionally long lifetimes [11]. These states are predicted to be preferentially populated by three-body recombination (TBR) in strongly magnetized cold plasmas [12]; this has recently been seen in the formation of antihydrogen in cold antiproton-positron plasmas [13]. TBR is a significant plasma heating mechanism which has frustrated efforts to realize a strongly coupled two-component plasma at low magnetic fields [14]. In strong magnetic fields, TBR and the associated plasma heating are predicted to be significantly suppressed [12], possibly allowing one to realize a strongly coupled two-component plasma in this regime. Additionally, by supplementing strong-magnetic-field neutral-atom traps with suitable electrodes, ion or electron

plasmas can simultaneously be confined in a Penning geometry at the same location as the trapped neutral atoms. The development of this interface is critical for the efforts to trap and study antihydrogen [13] and extends parallels with laser-cooled strongly coupled ions in Penning traps [15].

The cornerstone of our experiment is a custom-designed superconducting Ioffe-Pritchard magnet [16] with a liquid-helium cryopumped UHV interior and optical access along all three axes. The magnet, which consists of dipole and quadrupole coils as shown in Fig. 1(a), generates a magnetic field which near its center can be written

$$B(\mathbf{r}) \approx B_0 \left[1 + \frac{\beta^2 - \alpha}{2} (x^2 + y^2) + \alpha z^2 \right]. \quad (1)$$

The bias field B_0 at the trap center is oriented along the z axis and $B_0\alpha$ and $B_0\beta$ are the longitudinal curvature and transverse Ioffe gradient, respectively. The two large dipole coils provide the strong bias field $B_0 \leq 6.0$ T and are separated enough to produce longitudinal magnetic confinement ($\alpha = 2.2 \times 10^{-3} \text{ cm}^{-2}$ is fixed by the coil geometry). The quadrupole coils, which serve as the Ioffe bars, carry equal currents in opposite directions and provide transverse magnetic-field gradients $B_0\beta$ up to 0.75 T/cm in the absence of the bias field. Magnetic-trapping conditions are realized with simultaneous operation of the dipole and quadrupole coils; in our system, this mode of operation is possible up to $B_0 = 2.9$ T (with a trap depth of $\approx 0.03 \text{ T} \approx k_B/\mu_B \times 20 \text{ mK}$; k_B is Boltzmann's constant and μ_B is the Bohr magneton). Laser cooling without transverse confinement ($\beta = 0.0 \text{ T/cm}$) can be performed up to $B_0 = 6.0$ T.

The trap is loaded with a continuous accelerated cold atomic beam of ^{85}Rb from a pyramidal low velocity intense source (LVIS) [17] located 68 cm from the center of the superconducting trap, as indicated in Fig. 1. The water-cooled copper LVIS coils are driven independently in order to generate the necessary magnetic-field zero and modest

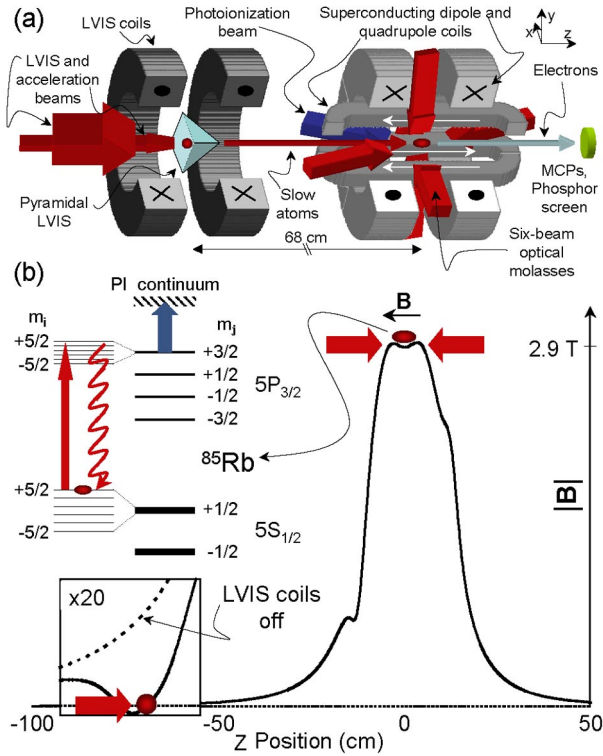


FIG. 1 (color online). (a) The pyramidal LVIS and strong-magnetic-field trap are shown schematically (the nearest sections of the magnets are cut out for clarity). (b) Magnetic field along the axis of the dipole coils for $B_0 = 2.9$ T, where the LVIS field has been scaled by $20 \times$. The strong-magnetic-field energy level scheme, laser cooling, and photoionizing transitions are shown at the upper left.

gradient (≈ 10 G/cm) in the tail of the superconducting magnet field for any B_0 . Atoms leaving the LVIS region are further accelerated by a narrowly focused ($500 \mu\text{m}$ beam waist) and slightly divergent laser beam aligned parallel to the atomic beam generated by the LVIS. This high intensity ($100\text{--}300 \text{ mW/cm}^2$) acceleration-laser beam is tuned to the blue ($\approx 10\text{--}25$ MHz) of the LVIS laser and is critical for the atoms in low-field-seeking states to reach sufficient velocity to climb the potential barrier presented by the strong magnetic field. At 6 T, a velocity larger than 28 m/s ($= \sqrt{2\mu_B B/M}$; M is the atomic mass) is required for ^{85}Rb . No loading is seen without this accelerating laser. In the LVIS and during the acceleration, atoms in the level $5S_{1/2}F=2$ are repumped to $5S_{1/2}F=3$ through $5P_{3/2}F'=3$ by optical sidebands on the trapping and accelerating beams [18]. The repumping also ensures that the atoms are in the low-field-seeking state $5S_{1/2}|F=3, m_F=+3\rangle = 5S_{1/2}|m_J=+1/2, m_I=+5/2\rangle$ when they enter the region of strong magnetic field.

Laser cooling in the superconducting atom trap is performed along all three axes by counterpropagating optical molasses beams, which are tuned slightly to the red of the

$5S_{1/2}|m_J=+1/2, m_I=+5/2\rangle \rightarrow 5P_{3/2}|m_J=+3/2, m_I=+5/2\rangle$ transition. Spontaneous decay repopulates the $5S_{1/2}|m_J=+1/2, m_I=+5/2\rangle$ state, making this a robust cycling transition. Optical pumping out of this cooling cycle is highly suppressed. At $B_0 = 3$ T and $I = I_{\text{sat}}$ ($I_{\text{sat}} \approx 1.6 \text{ mW/cm}^2$), scattering into the $5S_{1/2}|m_J=-1/2, m_I=+5/2\rangle$ state through the far-detuned $5P_{3/2}|m_J=+1/2, m_I=+5/2\rangle$ state occurs at an estimated rate of 10 mHz. Further, the relatively weak hyperfine interaction $\mathbf{I} \cdot \mathbf{J}$ offers a nonzero probability of making a transition to the $5P_{3/2}|+3/2, +3/2\rangle \leftrightarrow 5P_{3/2}|+1/2, +5/2\rangle$ state which is only 40 MHz redshifted from the laser-cooling transition. At $B_0 = 3$ T, $|\epsilon|^2 \approx 7 \times 10^{-7}$, leading to a scattering rate of 40 mHz into the state $5S_{1/2}|+1/2, +3/2\rangle$. These rates are low enough to allow significant atom accumulation in the target state without repumping.

Because of the large and variable Zeeman shift of the cooling transition relative to the field-free one (84 GHz at $B_0 = 6$ T), the molasses laser cannot be stabilized using conventional saturation spectroscopy. Instead, it is stabilized to within a few MHz using a homebuilt temperature-stabilized and pressure-tuned Fabry-Perot interferometer [19]. The six molasses beams have 6 mm FWHM, $0.6\text{--}30 \text{ mW}$ in total power, and are linearly polarized transverse to the magnetic field.

The cooled and trapped atoms are counted on a $\nu_{\text{rep}} = 10$ Hz cycle through two-step photoionization and electron detection, as indicated in Fig. 1(b). During a brief ($5 \mu\text{s}$) “probe” phase, the molasses light is blue shifted by 8 MHz and increased in intensity ($I \gg I_{\text{sat}}$) to maximize excitation to the $5P_{3/2}|m_J=+3/2, m_I=+5/2\rangle$ state. A coincident blue laser pulse (10 ns pulse width) is tuned a few meV above the ionization threshold ($\lambda < 479.1 \text{ nm}$) and is large enough to uniformly photoionize the $5P_{3/2}$ atoms in the trap. At a pulse energy of $\approx 0.3 \text{ mJ/pulse}$, the probability of ionizing a ground state atom was measured to be $P_{\text{ion}} \approx 1.6 \times 10^{-3}$ (see below). A constant electric field of 5 V/cm applied by electrodes around the trap region forces the electrons down the magnetic-field lines onto a double microchannel plate (MCP) and phosphor screen 47 cm away from trap center. A charge-coupled device (CCD) camera records the electron counts on the phosphor screen. The number of electrons N_e counted in a single-shot measurement depends on the number of atoms in the trap region as $N_e = \eta_{\text{col}} \eta_{\text{MCP}} P_{\text{ion}} N_a$, where η_{col} and η_{MCP} are the geometric collection efficiency and the MCP efficiency, respectively, and N_a is the atom number.

The steady-state spectral signature of atoms slowed and cooled from the atomic beam into the magnetic trap ($B_0 = 2.9$ T, $\beta B_0 = 0.32 \text{ T/cm}$) is shown by the filled dots in Fig. 2(a). A prominent peak, which is asymmetric and narrower than the natural linewidth, demonstrates the sensitive frequency dependence of laser cooling in the strong magnetic field. Simulations show that the steep, high-

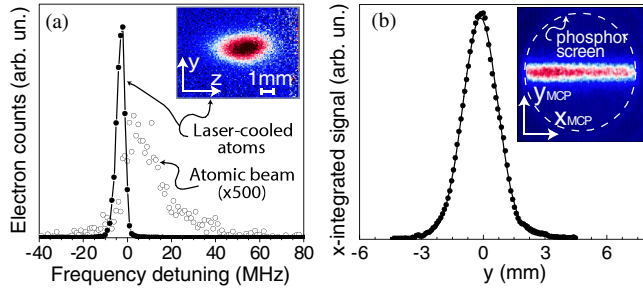


FIG. 2 (color online). (a) The number of photoelectrons obtained from trapped atoms (filled circles) and from the uncooled atomic beam (open circles, magnified 500 \times) vs probe frequency. The optical frequencies are referenced to the atomic transition at the trap center. The inset shows an optical image of the trap taken from a direction transverse to the magnetic field. (b) The x-integrated spatial profile of the atom cloud as a function of the y position (circles) and Gaussian fit (line) from a CCD image of electrons streamed onto the MCP and phosphor screen (inset).

energy side of the line coincides with zero detuning from resonance at the bottom of the trap. On the peak, 2.4×10^7 trapped atoms are counted as explained below. For comparison, a spectrum of the atomic beam—which is taken with the molasses laser switched off during the laser-cooling phase—is also shown in Fig. 2(a) (open dots, scale magnified 500 \times). As expected, the atomic-beam spectrum is characterized by a broad and weak peak at and above the transition frequency at the trap center.

The spatial distribution and temperature of the laser-cooled atomic cloud can be obtained by examining the image of the electrons generated through photoionization. Since the photoelectrons are tightly pinned to the magnetic-field lines that pass through the parent atoms, the photoelectrons maintain spatial information about the atom cloud as they stream down the magnetic-field lines and strike the MCP. An image of the electrons on the phosphor screen is shown in Fig. 2(b). The electron image of the atom cloud is magnified and elliptically distorted due to the magnetic-field decrease between the atom cloud and the MCP-phosphor screen and the lack of cylindrical symmetry of the quadrupole fields. Area densities of trapped atoms at atom-cloud coordinates (x, y) are obtained from signal densities measured at MCP-screen locations ($x_{\text{MCP}}, y_{\text{MCP}}$) using a mapping function ($x_{\text{MCP}}, y_{\text{MCP}}$) \rightarrow (x, y) that has been calculated for the given magnetic-field topology.

The temperature of the atom cloud can be obtained by integrating the atom area density along the x axis and examining the dependence of the resultant spatial distribution on y . For atoms at temperature T in the harmonic trap defined in Eq. (1), the spatial distribution along the transverse y dimension should take the form

$$n(y) = n_0 e^{-y^2/2\sigma_T^2} = n_0 e^{-\mu_B B_0 (\beta^2 - \alpha) y^2 / 2k_B T} \quad (2)$$

where σ_T is the transverse root-mean-square radius. The measured spatial distribution of atoms along the y axis, shown by circles in Fig. 2(b), is fit by Eq. (2) (line), revealing $\sigma_T = 0.84$ mm and a transverse temperature $T_T \approx 140$ μ K. An optical image of the trap fluorescence, shown in Fig. 2(a), yields $\sigma_T = 0.80$ mm and $\sigma_L = 1.5$ mm which corresponds to $T_T \approx 125$ μ K and $T_L \approx 185$ μ K, respectively, where σ_L and T_L are the longitudinal root-mean-square radius and temperature. Therefore, the trapped atoms are cooled to near the Doppler limit (140 μ K). The atom number and trap size measurements yield atom densities of 2×10^9 cm $^{-3}$.

Important measures for the performance of optical molasses and atom traps are loading times and lifetimes. Typical loading and lifetime curves are shown in Fig. 3(a) for the molasses in the Ioffe-Pritchard trap with $B_0 = 2.9$ T, $\beta B_0 = 0.32$ T/cm, and $I = 1.6$ mW/cm 2 . The loading curve for the initially empty trap, shown by the filled circles, is obtained by turning on the acceleration-laser beam at $t = 0$ and reveals a loading rate on the order of 10^6 s $^{-1}$. Based on estimates of velocities and densities of the atoms passing through the trap region (10 m/s and 10^5 cm $^{-3}$, respectively), we deduce a capture efficiency for these atoms on the order of a few percent. Lifetime curves showing the number of atoms remaining in an initially filled molasses are obtained by turning off the LVIS at $t = 0$. The lifetime curve displayed in Fig. 3(a) by open circles is well fit by an exponential with a decay time of $\tau_{\text{mol}} = 10$ s. Trap loss on this time scale could be due to the optical pumping mechanisms into untrapped or dark states discussed above.

Once atoms are laser cooled in a magnetic field with 3D confinement, the optical fields can be turned off and, in accordance with the measured low temperature, nearly 100% of the laser-cooled atoms remain magnetically trapped. The large open circles in Fig. 3(b) show the number of atoms remaining in the magnetic trap after a time t , where the molasses laser is turned off at $t = 0$ and

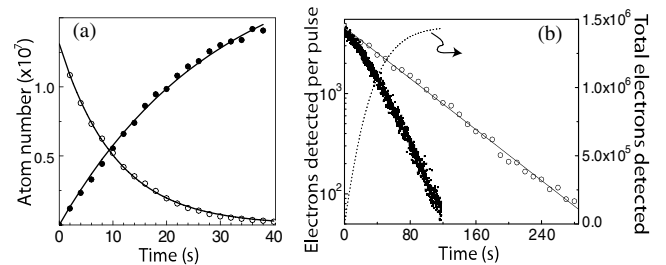


FIG. 3. (a) Loading (filled circles) and lifetime (open circles) curves for optical molasses in the 2.9 T Ioffe-Pritchard trap. (b) Number of electrons detected as a function of delay time after loading when photoionizing pulses are applied at 10 Hz (small filled circles, left axis), supplemented with the running sum (dotted line, right axis) in order to count the magnetically trapped atoms. Measurement at 0.1 Hz (open circles, left axis) provides a trap lifetime. Solid line is a linear fit.

the atoms are probed every 10 s. In this case, the trap depletion due to the photoionization is negligible. An exponential fit to the data yields a decay rate $\gamma_{bg} = (71 \text{ s})^{-1}$, consistent with a background pressure in the 10^{-10} Torr range.

The number of atoms in the magnetic trap is determined by the application of photoionizing pulses at a repetition rate of $\nu_{rep} = 10$ Hz and accumulation of the total number of detected photoelectrons, N_e^{sum} . Evaluation of Fig. 3(b) yields a total trap decay rate of $\gamma \approx (33 \text{ s})^{-1}$ and $N_e^{sum} = 1.4 \times 10^6$. Noting that $\gamma = \gamma_{bg} + \nu_{rep} P_{ion}$, a single-pulse photoionization probability $P_{ion} \approx 1.6 \times 10^{-3}$ is deduced. The fraction of atoms removed from the trap by photoionization (and not by background gas collisions) is found to be $\eta_{PI} = \nu_{rep} P_{ion} / \gamma \approx 0.53$. From the fit to the image in Fig. 2(b) and the corresponding mapping function $(x, y) \rightarrow (x_{MCP}, y_{MCP})$, the geometrical photoelectron collection efficiency was determined to be $\eta_{col} = 0.28 \pm 0.03$. The electron detection efficiency of the MCP is assumed to be $\eta_{MCP} = 0.4 \pm 0.1$. The number of magnetically trapped atoms at $t = 0$ then is $N_a = N_e^{sum} / (\eta_{PI} \eta_{col} \eta_{MCP}) = (2.4 \pm 0.7) \times 10^7$.

Leaving the quadrupole coils off ($\beta = 0.0$ T/cm), we have slowed and laser-cooled atoms in bias fields up to $B_0 = 6$ T. In this mode of operation, the efficiency is reduced due to the negative curvature of the magnetic field along the transverse axes [as seen by Eq. (1)], which prevents magnetic trapping and limits the optical molasses lifetime to 10's of ms. At $B_0 = 6$ T, we have maintained 2×10^5 atoms in a 30 mW continuous molasses. Using a pulsed atomic beam to load the molasses, we have achieved peak atom numbers of 3×10^6 and densities of $4 \times 10^7 \text{ cm}^{-3}$.

In summary, we have performed laser cooling in variable bias magnetic fields up to $B_0 = 6.0$ T and achieved magnetic trapping up to $B_0 = 2.9$ T in a superconducting Ioffe-Pritchard trap. We are currently exploring the field ionization of Rydberg atoms at fields up to $B_0 = 6.0$ T. Utilizing the higher densities and lower temperatures available at $B_0 = 2.9$ T, we investigate collisions in cold Rydberg gases and TBR in cold plasmas. We are also characterizing the properties of the Ioffe-Pritchard neutral-atom trap combined with a Penning trap for charged particles [20]. To date, the system described in this letter is the only one capable of trapping both neutral and charged particles at the same point in space.

The authors would like to thank P.H. Bucksbaum and D.G. Steel for the generous loaning of equipment. This

work was supported by the Chemical Sciences, Geosciences, and Biosciences Division of the Office of Basic Energy Sciences, Office of Science, U.S. Department of Energy.

*Present address: Physics Division, Argonne National Laboratory, Argonne, IL 60439, USA

- [1] E. A. Cornell and C. E. Wieman, *Rev. Mod. Phys.* **74**, 875 (2002).
- [2] J. Weiner, V. S. Bagnato, S. Zilio, and P. S. Julienne, *Rev. Mod. Phys.* **71**, 1 (1999).
- [3] S. Gupta, K. Dieckmann, Z. Hadzibabic, and D. E. Pritchard, *Phys. Rev. Lett.* **89**, 140401 (2002).
- [4] T. C. Killian *et al.*, *Phys. Rev. Lett.* **83**, 4776 (1999); M. P. Robinson *et al.*, *Phys. Rev. Lett.* **85**, 4466 (2000); T. C. Killian *et al.*, *Phys. Rev. Lett.* **86**, 3759 (2001); S. K. Dutta *et al.*, *Phys. Rev. Lett.* **86**, 3993 (2001); A. Walz-Flannigan, J. R. Guest, J.-H. Choi, and G. Raithel, *Phys. Rev. A* **69**, 063405 (2004).
- [5] H. J. Metcalf, *NBS Spec. Publ. (U.S.)* **653**, 59 (1983).
- [6] J. J. Tollett, C. C. Bradley, C. A. Sackett, and R. G. Hulet, *Phys. Rev. A* **51**, R22 (1995).
- [7] V. S. Bagnato *et al.*, *Phys. Rev. Lett.* **58**, 2194 (1987); K. Helmerson, A. Martin, and D. E. Pritchard, *J. Opt. Soc. Am. B* **9**, 1988 (1992).
- [8] J. Kim *et al.*, *Phys. Rev. Lett.* **78**, 3665 (1997).
- [9] H. Friedrich and D. Wintgen, *Phys. Rep.* **183**, 37 (1989), and references therein.
- [10] J. R. Guest and G. Raithel, *Phys. Rev. A* **68**, 052502 (2003).
- [11] J. R. Guest, J.-H. Choi, and G. Raithel, *Phys. Rev. A* **68**, 022509 (2003).
- [12] M. E. Glinsky and T. M. O'Neil, *Phys. Fluids B* **3**, 1279 (1991).
- [13] M. Amoretti *et al.*, *Nature (London)* **419**, 456 (2002); G. Gabrielse *et al.*, *Phys. Rev. Lett.* **89**, 213401 (2002).
- [14] F. Robicheaux and J. D. Hanson, *Phys. Rev. Lett.* **88**, 055002 (2002).
- [15] T. B. Mitchell *et al.*, *Science* **282**, 1290 (1998).
- [16] The superconducting magnet was built by American Magnetics and installed in a liquid-helium dewar by Janis Research.
- [17] Z.-T. Lu *et al.*, *Phys. Rev. Lett.* **77**, 3331 (1996).
- [18] C. J. Myatt, N. R. Newbury, and C. E. Wieman, *Opt. Lett.* **18**, 649 (1993).
- [19] E. Hansis *et al.*, (to be published).
- [20] T. M. Squires, P. Yesley, and G. Gabrielse, *Phys. Rev. Lett.* **86**, 5266 (2001); E. P. Gilson and J. Fajans, *Phys. Rev. Lett.* **90**, 015001 (2003).